NASA-CR-197- 206375 Final NAG3-1716

OCIT.
102584

DETERMINATION OF RESIDUAL STRESS IN COMPOSITE MATERIALS USING ULTRASONIC WAVES

Principal Investigator: S. I. Rokhlin

The Ohio State University

Nondestructive Evaluation Program

1248 Arthur Adams Drive

Columbus, Ohio 43221

NASA Contract # NAG3-1716

Abstract

The performance of high temperature composites can be significantly affected by the presence of residual stresses. These stresses arise during cooling process from fabrication to room temperature due to mismatch of thermal expansion coefficients between matrix and fiber materials. This effect is especially pronounced in metal matrix and intermetallic composites. It can lead to plastic deformations, matrix cracking and fiber/matrix interface debonding. In this work the feasibility of ultrasonic techniques for residual stress assessment in composites is addressed. A novel technique for absolute stress determination in orthotropic materials from angular dependencies of ultrasonic velocities is described. The technique is applicable for determination of both applied and residual stresses and does not require calibration measurements on a reference sample. The important advantage of this method is that the stress is determined simultaneously with stress-dependent elastic constants and is thus decoupled from the material texture. It is demonstrated that when the principal plane stress directions coincide with acoustical axes, the angular velocity data in the plane perpendicular to the stress plane may be used to determine both stress components. When the stress is off the acoustical axes, the shear and the difference of the normal stress components may be determined from the angular dependence of group velocities in the plane of stresses. Synthetic sets of experimental data corresponding to materials with different anisotropy and stress levels are used to check the applicability of the technique. The method is also verified experimentally. A high precision ultrasonic wave transmission technique is developed to measure angular dependence of ultrasonic velocities. Examples of stress determination from experimental velocity data are given. A method is presented for determination of velocities of ultrasonic waves propagating through the composite material with residual stresses. It is based

on the generalized self-consistent multiple scattering model. Calculation results for longitudinal and shear ultrasonic wave velocities propagating in the perpendicular to fibers direction in SCS-6/Ti composite with and without residual stresses are presented. They show that velocities changes due to presence of stresses are of order 1%.

Contents

Chapter 1

MODELING OF WAVE PROPAGATION IN STRESSED MATERIALS

1.1 Introduction

The characteristic dependence of ultrasonic velocity on stress has long been thought promising for residual stress measurements in materials. Reviews of the theory and experimental methods have been given by Pao et al. [1], Cantrell and Salama [2] and Thompson et al. [3]. The major problem in the practical utilization of most of these techniques is the necessity of separating the effects of texture (anisotropy) and stress on the measured ultrasonic velocity. In most cases the materials under consideration have unknown anisotropy and even if the anisotropy is small its effect cannot be neglected in stress measurements.

A few methods have been proposed to overcome this difficulty. Thompson et

al. [6] considered the difference of two SH-waves propagating in the plane of the material in orthogonal directions. They showed that for this difference the effect of anisotropy is reduced by an order of magnitude and for small anisotropy it can be neglected. Also they demonstrate that the stress and anisotropy terms have different angular dependencies which can be used for their separation. King and Fortunko [4] considered obliquely incident SH-waves. Again a formula was derived with separate anisotropic and stress terms. Man and Lu [7] generalized both techniques and demonstrated the applicability of the ultrasonic method for stress measurements in materials which had undergone a complicated (possibly plastic) history of loading and unloading.

Recently we proposed [9] a different approach. We showed that the stresses in an anisotropic material can be found simultaneously with the stress-dependent elastic constants from an inversion of the Christoffel equation, using as input measured angular dependencies of bulk wave velocities. The method is applicable for determination of both applied and residual stresses for materials of the most general loading histories. In this paper we will further explore this method and show that the absolute error in stress determination using this technique is independent of the degree of anisotropy and the stress level is defined only by the accuracy of wave velocity measurement. The feasibility of the experimental application of this technique is also demonstrated. Since velocity changes due to stress are small (typically below 0.1%) a very precise measurement of the ultrasonic velocity is required. We discuss modifications of the experimental technique described by Rokhlin and Wang [13] and Chu and Rokhlin [16] to achieve higher precision. As an example experimental results are presented for stress determination in plexiglass.

1.2 Theory of the absolute stress determination method

To describe wave propagation in a prestressed medium we consider the prestressed configuration as the reference configuration where the initial stress is accounted for in the Christoffel equation for an anisotropic material under stress:

$$[C_{ijkl}n_in_l + (\sigma_{il}n_in_l - \rho V^2)\delta_{jk}]p_k = 0 \tag{1.1}$$

Eq. (1.1) was derived by Tokuoka and Iwashimizu [8] and used by Thompson et al. [6] and King and Fortunko [4]. Man and Lu [7] reexamined constitutive equations and extended the applicability of Eq. (1.1) to general types of loading history, including plastic deformations. The difference of Eq. (1.1) from the Christoffel equation in an unstressed medium is the appearance of stress dependent elastic constants C_{ijkl} instead of second order elastic constants C^o_{ijkl} and the addition of the stress term $\sigma_{il}n_in_l$ in the diagonal elements. The effect of the stress term on the wave velocity can be isolated.

Two cases of principal stress orientation with respect to material axes of symmetry will be considered. In the first case we consider the principal stress axes oriented along symmetry axes 1-2 of the material (Fig. 1.1) and wave propagation in symmetry planes 1-3 and 2-3, i.e., perpendicular to the stress plane 1-2. The second case is the general plane stressed state, i.e. when principal directions deviate from symmetry axes (Fig. 1.2). Here we utilize waves propagating and polarized in the plane of stress (1-2 plane).

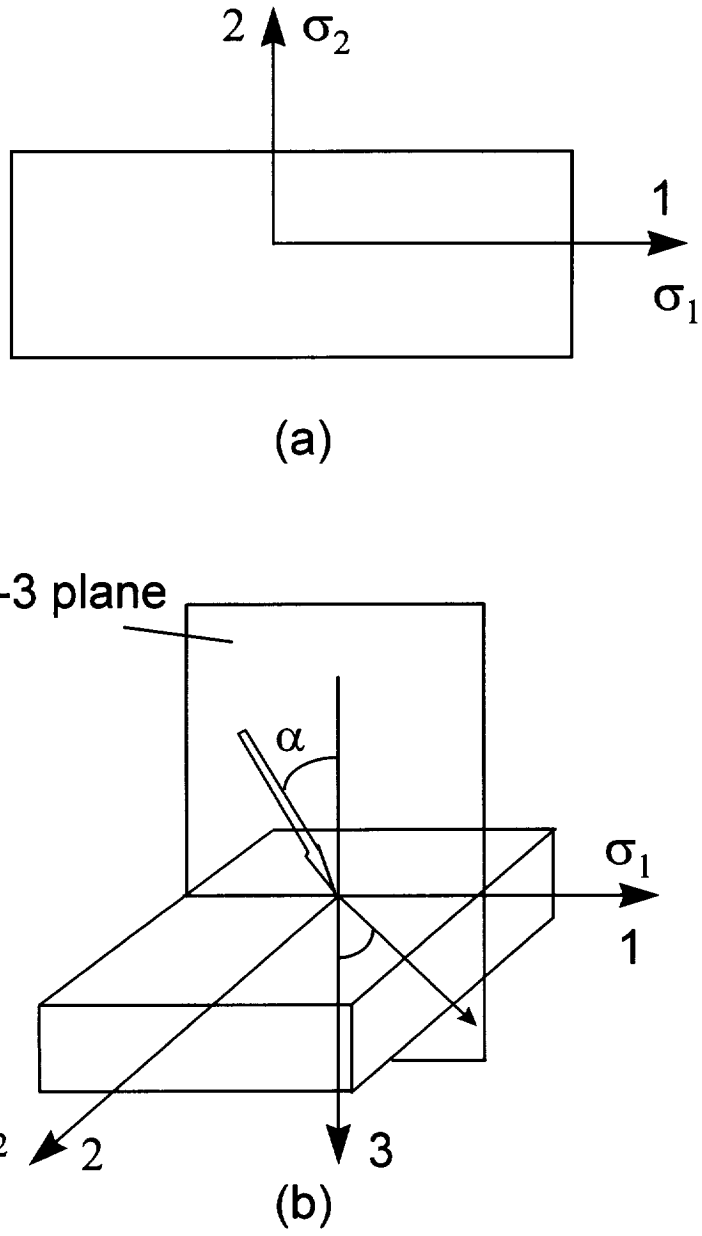

Figure 1.1: (a) Plane stress state, principal stress directions coincide with acoustical axes. (b) Wave propagation planes (1-3 and 2-3 symmetry planes) are perpendicular to the principal stress plane (1-2 symmetry plane)

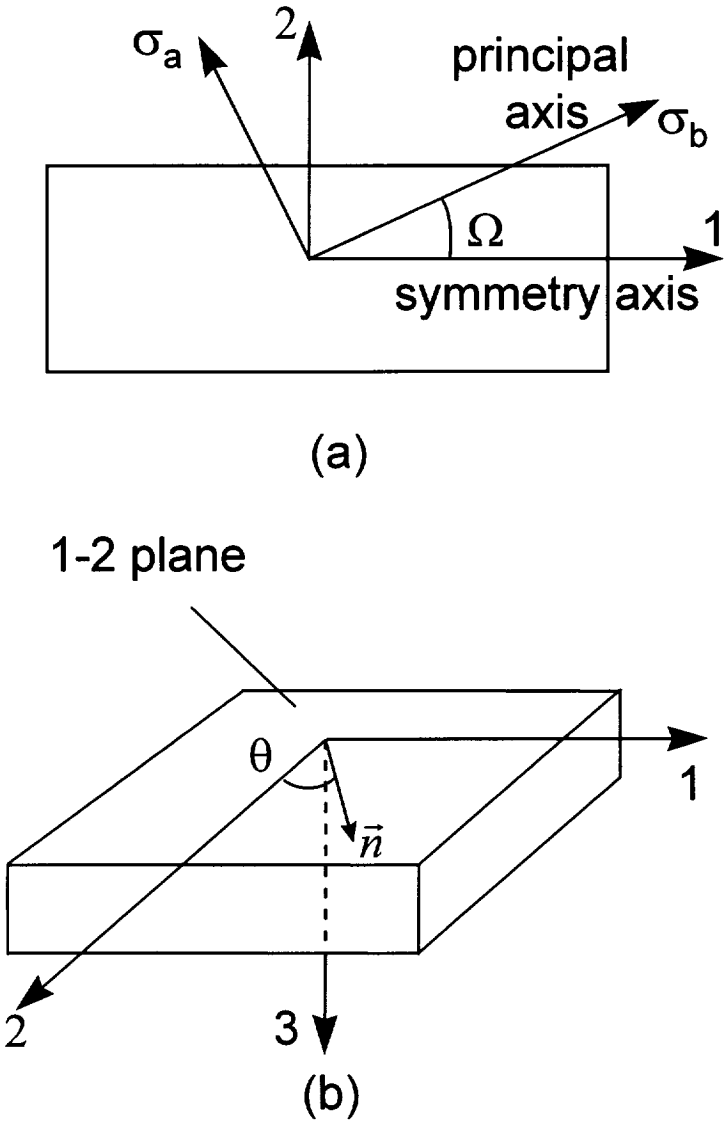

Figure 1.2: (a) Plane stress state, principal stress deviate from acoustical axes. (b) Wave propagation plane coincide with stress plane (1-2 symmetry plane)

1.2.1 Principal stresses along symmetry axes. Wave propagation perpendicular to the stress plane

Let us consider plane stress in the 1-2 plane with the shear stress component σ_{12} being zero and wave propagation in the 1-3 or 2-3 symmetry planes (see Fig. 1.1). When principal axes coincide with symmetry axes of an orthotropic material, the stresses do not change the symmetry and the number of independent effective elastic constants C_{ijkl} in the stressed solid is the same as the number of second order elastic constants C^o_{ijkl}, which is nine.

For wave propagation in the 1-3 plane the Christoffel equation (1.1) has the following form:

$$\begin{vmatrix} G_{11} - (\rho V^2 - \sigma_{11}s^2) & 0 & G_{13} \\ 0 & G_{22} - (\rho V^2 - \sigma_{11}s^2) & 0 \\ G_{13} & 0 & G_{33} - (\rho V^2 - \sigma_{11}s^2) \end{vmatrix} = 0 \qquad (1.2)$$

where

$$\begin{aligned} G_{11} &= C_{11}s^2 + C_{55}c^2; \quad & G_{33} &= C_{55}s^2 + C_{33}c^2; \\ G_{13} &= (C_{13} + C_{55})sc; \quad & G_{22} &= C_{66}s^2 + C_{44}c^2; \\ s &= \sin\theta; \quad & c &= \cos\theta. \end{aligned} \qquad (1.3)$$

θ is the angle between the wave normal and the 3-axis [Fig. 1.1(b)]. Eq. (1.2) can be decoupled leading to simple closed-form solutions for phase velocities:

$$\begin{aligned} \rho V^2_{QL} &= \frac{G_{11} + G_{33}}{2} + \frac{\sqrt{(G_{11} - G_{33})^2 + 4G^2_{13}}}{2} + \sigma_{11}s^2 \\ \rho V^2_{QT} &= \frac{G_{11} + G_{33}}{2} - \frac{\sqrt{(G_{11} - G_{33})^2 + 4G^2_{13}}}{2} + \sigma_{11}s^2. \end{aligned} \qquad (1.4)$$

Here QL and QT denote quasilongitudinal and quasitransverse waves, respectively. Both these waves are polarized in the 1-3 plane. As one can see the QL and QT

phase velocities in this symmetry plane depend on only five parameters, namely $C_{11}, C_{33}, C_{13}, C_{55}$ and σ_{11}. Similarly, QL and QT phase velocities in the 2-3 plane depend on four stress dependent elastic constants $C_{22}, C_{33}, C_{23}, C_{44}$ and the stress component σ_{22}. The formulas for velocities in this plane can be obtained from Eqs. (1.2,1.4) by permuting indices 1 and 2.

1.2.2 Principal stresses off symmetry axes. Wave propagation in the plane of stresses

Now let us consider an arbitrary plane stress state in the 1-2 plane [Fig. 1.2(a)] of an orthotropic material; σ_{11}, σ_{22} and σ_{12} are the only nonzero stress components. In this case the symmetry reduces to monoclinic and the matrix of stress dependent elastic constants C_{ij} takes the following form:

$$[C_{ij}] = \begin{bmatrix} C_{11} & C_{12} & C_{13} & 0 & 0 & C_{16} \\ C_{12} & C_{22} & C_{23} & 0 & 0 & C_{26} \\ C_{13} & C_{23} & C_{33} & 0 & 0 & C_{36} \\ 0 & 0 & 0 & C_{44} & C_{45} & 0 \\ 0 & 0 & 0 & C_{45} & C_{55} & 0 \\ C_{16} & C_{26} & C_{36} & 0 & 0 & C_{66} \end{bmatrix}. \tag{1.5}$$

$C_{16}, C_{26}, C_{36}, C_{45}$ are stress-induced effective elastic constants depending only on the shear stress component σ_{12} (for unstressed orthotropic material these are zero).

If $\sigma_{12} \neq 0$ then the solution of the Christoffel equation in the 1-3 plane cannot be represented in the form of Eq. (1.4) because this shear stress component alters the material symmetry and the 1-3 plane becomes the nonsymmetry plane. As has been discussed by Chu [15] the reconstruction of elastic constants from phase velocities in a nonsymmetry plane is unstable. Our simulation reveals similar behavior for stress

determination. Even very small scatter in the velocity data destabilizes the inversion process for the stress.

These difficulties could be overcome if instead of considering wave propagation in planes orthogonal to the stress plane, we consider the wave propagation in the plane of the stresses [Fig. 1.2(b)]. This plane still remains the plane of symmetry and the Christoffel equation (1.1) can again be decoupled. The solutions for quasilongitudinal and quasishear (polarized in the stress plane) waves have the following form:

$$\begin{aligned} \rho V_{QL}^2 &= \frac{G_{11}+G_{22}}{2} + \frac{\sqrt{(G_{11}-G_{22})^2+4G_{12}^2}}{2} + (\sigma_{11}-\sigma_{22})s^2 + \sigma_{22} + 2\sigma_{12}sc \\ \rho V_{QT}^2 &= \frac{G_{11}+G_{22}}{2} - \frac{\sqrt{(G_{11}-G_{22})^2+4G_{12}^2}}{2} + (\sigma_{11}-\sigma_{22})s^2 + \sigma_{22} + 2\sigma_{12}sc, \end{aligned} \tag{1.6}$$

where

$$G_{11} = C_{11}s^2 + C_{66}c^2 + 2C_{16}sc; \qquad G_{12} = (C_{12}+C_{66})sc + C_{16}s^2 + C_{26}c^2;$$

$$G_{22} = C_{66}s^2 + C_{22}c^2 + 2C_{26}sc; \qquad s = \sin\theta; \qquad c = \cos\theta.$$

1.2.3 Inversion procedure

From the measured angular velocity dependencies in the 1-3 or 2-3 plane, assuming that the principal stress directions of the plane stress coincide with acoustical axes (Fig. 1.1), we can determine five unknown parameters (four elastic constants and the stress component which lies in the wave propagation plane). We employ the least squares method for the minimization of the sum of squared deviations between experimental and calculated velocities considering the effective elastic constants and the stress component as variables in a multidimensional space:

$$\min_{C_{ij},\sigma_{ij}\in\Re^n} \frac{1}{2}\sum_{i=1}^{m}(V_i^e - V_i^c)^2 \tag{1.7}$$

Here m is the number of velocity data points for different directions, and V^e and V^c are the experimental and calculated phase velocities, respectively. This approach was used [14, 15] to find second order elastic constants from velocity data in symmetry and nonsymmetry planes for orthotropic materials.

The flow chart of the inversion procedure for the 1–3 plane is presented in Fig. 1.3. Four stress dependent elastic constants ($C_{11}, C_{33}, C_{13}, C_{55}$) and one stress component (σ_{11}) form a 5-dimensional space of unknown parameters. By selecting a set of initial guesses for these parameters the velocities of the QL and QT waves are calculated and the unknown parameters are determined by minimization of the sum of squared differences from Eq. (1.7) between the experimental and calculated velocities at different propagation angles.

When the reconstruction is performed from the velocity date in both 1–3 and 2–3 planes, both stress components σ_{11} and σ_{22} and seven of the nine stress dependent elastic constants (all except C_{12} and C_{66}) are found.

When principal stress directions deviate from acoustical axes and we have velocity data in the plane of the sample (Fig. 1.2) the inversion procedure in the space of unknowns $C_{11}, C_{22}, C_{12}, C_{66}, C_{16}, C_{26}, \sigma_{11}, \sigma_{22}, \sigma_{12}$ is used. The simulations show that the difference of normal stresses ($\sigma_{11} - \sigma_{22}$) and the shear stress σ_{12} can be determined using the inversion procedure described above and the solution is stable. If we consider the uniaxial stress Σ, applied at the angle Ω (considered unknown) to the 1-axis then the value of this stress and the angle Ω can be obtained as:

$$\Omega = \frac{1}{2}\tan^{-1}\left(\frac{2\sigma_{12}}{\sigma_{11} - \sigma_{22}}\right) \tag{1.8}$$

$$\Sigma = (\sigma_{11} - \sigma_{22})\cos 2\Omega + 2\sigma_{12}\sin 2\Omega. \tag{1.9}$$

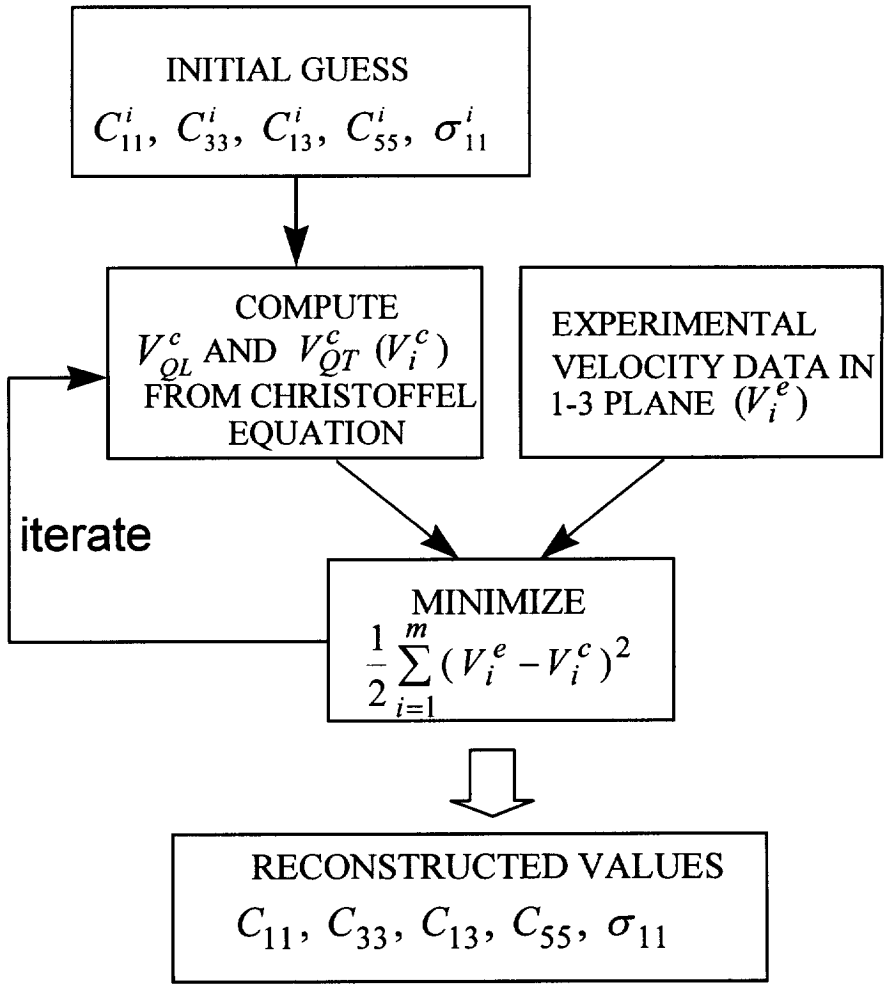

Figure 1.3: Flow chart for determination of the stress and stress dependent elastic constants from velocity angular dependence in 1–3 plane.

1.3 Effect of stress level and anisotropy on the accuracy of stress reconstruction

To validate our approach by computer simulation we need to create a set of synthetic data. To do this we compute the stress-dependent elastic constants C_{ijkl} as a function of stress, considering a finitely stressed hyperelastic body and assuming the second and third order elastic constants known. While the velocity data set thus generated is for hyperelastic material, our process for determination of stress using Eq. (1.1) does not have this limitation and has the same applicability as Eq. (1.1) itself. Stress dependent elastic constants can be calculated from second and third order elastic constants and stresses. The detailed computational procedure is given in [9]. From the known material properties (density, second and third order elastic constants) and the plane stressed state which we assume to result from elastic deformation we generate synthetic sets of phase velocity data $\{V_p^{exp}(\theta^{exp})\}$. To simulate the effect of experimental error we use a random function generator to introduce scatter of different levels in the velocity data.

To determine the accuracy of the inversion procedure, values of stresses and stress dependent elastic constants C_{ij} were found for different materials and stress levels and compared with those originally selected for the velocity data generation.

As the first example let us consider principal stresses along the symmetry axes in the 1-2 plane, with velocity data in the 1-3 and 2-3 planes. Ultrasonic velocities in the plane of symmetry, let us say in the 1-3 plane, will be affected by both in-plane (σ_{11}) and orthogonal-to-the-plane (σ_{22}) stress components. However our results show that the orthogonal stress does not affect the value of the in-plane stress reconstructed from the velocities in this plane. Thus, for example, the correct value of σ_{11} is determined

independently of σ_{22}, from the velocities in the 1-3 plane. For this reason, without limitation of generality, we consider an example of uniaxial stress (σ_{11}) determination from velocity data in the 1-3 plane.

One example considered is for textured aluminum with anisotropy of 1%. The third order elastic constants were taken from the handbook [10] for isotropic aluminum. As the second example computations were made for a graphite/epoxy composite which exhibits strong orthotropy. The third order elastic constants were chosen arbitrarily assuming only that they are approximately one order of magnitude greater than the second order elastic constants. It was observed that a different choice of third order elastic constants did not affect the accuracy of the reconstruction process.

The computations were performed at different stress levels (0 – 300 MPa) and different scattering (0 – 0.1%). As an initial guess for the effective elastic constants we select the second order elastic constants at zero stress and as the initial guesses for stress we select zero. The results do not depend on the initial guesses. For each value of stress and scattering level 50 runs were made and the standard deviations for reconstructed elastic constants and stresses were computed. Results for stress are presented in Table I. The results for the aluminum are in columns (a) and for the graphite/epoxy are in columns (b).

Comparing the results for weakly anisotropic (textured aluminum) and strongly anisotropic (graphite/epoxy composite) materials we conclude that the accuracy of the stress reconstruction does not depend on the degree of anisotropy. Also for each scattering level we have approximately the same absolute error in stress determination regardless of the stress level.

Table I: Standard deviations for the reconstructed uniaxial (σ_{11}) stress determined from velocity data in the 1-3 plane for (a) textured aluminum and (b) graphite/epoxy composite samples. Standard deviation is computed for different stress levels using 50 runs with different levels of velocity data scatter.

Original value σ_{11}, MPa	Standard deviation of the reconstructed σ_{11} value from the original, MPa							
	no scatter		0.01 % scatter		0.05 % scatter		0.1 % scatter	
	a	b	a	b	a	b	a	b
0	0	0	5	5	15	22	48	39
100	0	0	5	5	24	20	36	56
200	0	0	4	6	26	27	49	56
300	0	0	5	6	25	28	40	56
400		0		4		24		51
500		0		4		23		54

1.4 Conclusions

An approach for absolute stress determination from the angular dependence of the ultrasonic velocities has been described. It is based on inversion of the Christoffel equation in a multidimensional space formed by the stress dependent elastic constants and the stress components. The technique is applicable for determination of both applied and residual stresses. In the case when the principal plane stress directions coincide with symmetry axes of the orthotropic material, one can reconstruct the principal stresses from the angular dependence of quasilongitudinal and quasishear waves measured in these planes. When the principal axes do not coincide with symmetry axes the angular dependence of quasilongitudinal and quasishear waves propagating and polarized in the plane of stresses can be used to determine the shear stress and the difference between the normal stresses. Numerical simulation using a set of synthetic velocity data show that the reconstructed stress values are not affected by the selection of the initial guesses and that the absolute error in stress determination does not depend on the stress level and the degree of the material anisotropy or texture.

Chapter 2

EXPERIMENTAL VERIFICATION OF ABSOLUTE STRESS MEASUREMENT TECHNIQUE

2.1 Self-Reference Bulk Wave (SRBW) Method for Phase Velocity Measurement

To measure the angular dependence of the ultrasonic bulk wave velocity we used a Self-Reference Bulk Wave (SRBW) method developed in our laboratory [13, 16] for determination of elastic moduli of composites.

The basic idea of this method is illustrated in Fig. 2.1 where the directions of the ultrasonic path are shown for an anisotropic sample immersed in fluid. Two steps are required. First, the time for one ultrasonic wave reverberation inside the sample in

the normal direction, t_0, is measured. This is twice the time of wave travel through the sample and thus the corresponding wave velocity V_n is calculated using the known thickness h of the sample: $V_n = 2h/t_0$. Second, the total times of flight (through water and sample) t_{θ_i} for arbitrary oblique incidence at angles θ_i are measured. Due to the acoustic path length change in the sample, the time-delay difference Δt_{θ_i} between t_{θ_i} and the reference time of flight t_n at normal incidence is obtained ($\Delta t_{\theta_i} = t_n - t_{\theta_i}$) and used for phase velocity calculation.

For a generally anisotropic material, the phase velocities at refraction angle θ_r (corresponding to the incident angle θ_i shown in Fig. 2.1) are calculated using the phase velocity in the normal direction V_n and the time-delay change Δt_{θ_i} for the rotated sample

$$V_{\theta_i}(\theta_r) = \left(\frac{1}{V_n^2} + \frac{\Delta t_0 - (\Delta t_0 + \Delta t_{\theta_i}) \cos\theta_i}{h V_0} + \frac{\Delta t_{\theta_i}(2\Delta t_0 + \Delta t_{\theta_i})}{4h^2} \right)^{-1/2} \tag{2.1}$$

with

$$\theta_r = \sin^{-1} \frac{V_{\theta_i} \sin\theta_i}{V_0}. \tag{2.2}$$

Here V_0 is the sound speed in water, h is the thickness of the sample, and $\Delta t_0 = 2h(1/V_0 - 1/V_n)$. The phase velocity at normal incidence is measured by overlapping multiply reflected signals from the front and back surfaces of the sample. Since all measurements are made relative to the reference acoustic path in the presence of the sample, the effect of geometric imperfections is significantly reduced [16]. Ultrasonic measurements are made in the computer-controlled goniometer with angle resolution and repeatability better than 0.01 deg.

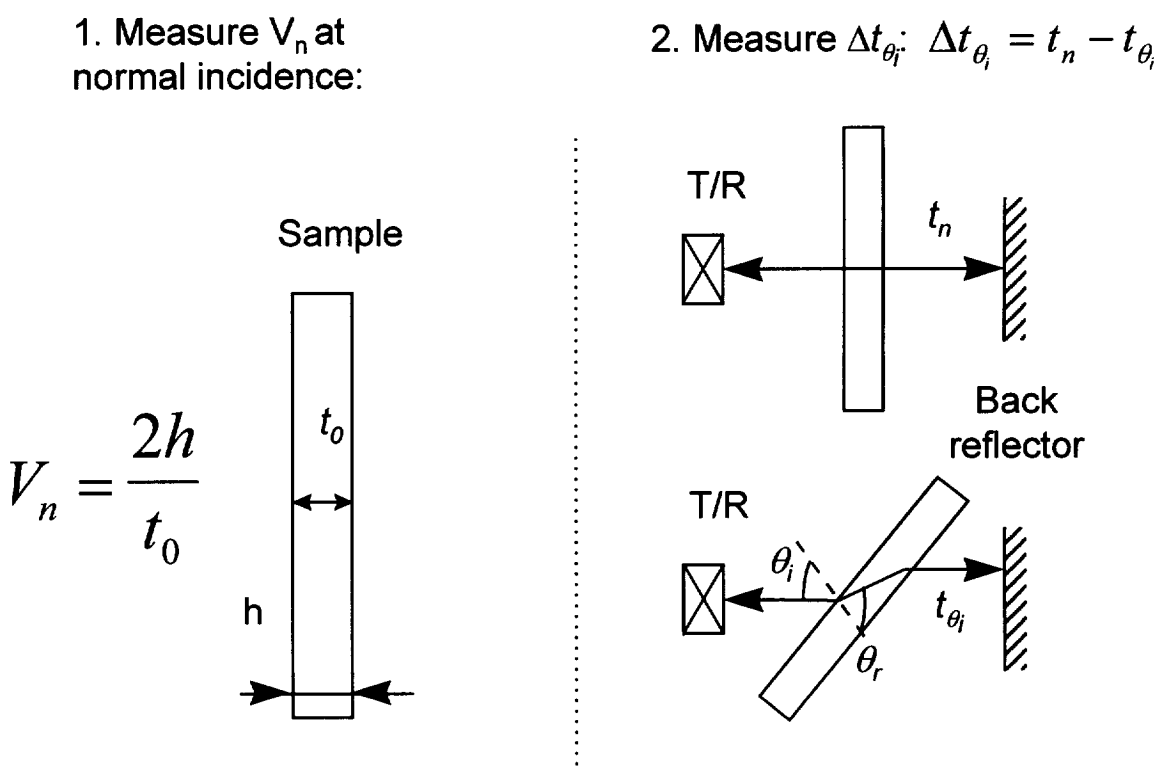

Figure 2.1: Schematic diagram of the self-reference bulk wave method.

2.2 Improvements of the method accuracy

For experimental stress measurement one needs to improve the precision of the SRBW method. The precision of $V_{\theta_i}(\theta_r)$ measurement was enhanced by increasing the precision of the parameter measurements in Eq. (2.1): $h, V_0, V_n, \Delta t_{\theta_i} = t_n - t_{\theta_i}$.

The thickness of the sample is measured by a micrometer with $\pm 2\,\mu m$ precision, which for a 10 mm thick specimen corresponds to .02% relative error. When a known external stress is applied to a specimen, the Poisson thickness change is evaluated (from the known applied stress, specimen thickness and Poisson ratio) and subtracted from the thickness measured at zero stress.

The sound speed in water V_0 depends on the water temperature which is maintained constant during experiment with precision ± 0.04°C. A slow temperature drift during measurement time is taken into account by measuring it with a J-type thermocouple (iron-constantan) at each data point. At 30°C (the usual temperature in our experiments) the corresponding precision of the determination of the speed in water is $\approx 0.1\,m/sec$ (.007% relative error).

Previously (for elastic constant determination purposes), the phase velocity in the specimen at normal incidence V_n was measured by overlapping multiply reflected signals from the front and back surfaces of the sample. The following modifications were made to improve the precision of V_n measurement:

1. A tone-burst signal with a narrow spectrum (instead of a broad band pulse) was used. This significantly decreases signal shape distortion due to dispersion and frequency dependent attenuation of the signals traveling different distances inside the specimen. The time delay between signals was measured using corresponding zero-crossing points thus eliminating the need for signal amplitude

adjustments in the overlapping technique.

2. When measuring the time delay between two multiple-reflection signals, we use the zero-crossing point of the first as a trigger for a digital oscilloscope. This automatically eliminates any signal instability due to water temperature fluctuations and system component vibrations. In addition, the highest possible oscilloscope time resolution can be utilized (up to 20 psec per point).

To improve the precision of the transmission time measurement t_{θ_i} at oblique incidence we introduced the second ultrasonic transducer (Fig. 2.2). The signal from the first transducer (tone-burst) goes through both water and the sample and the signal from the second transducer (pulse) goes through only the water. The length of the path through the water is similar for both signals. The signal from the second transducer is used for oscilloscope triggering to measure the first signal time delay. Thus signal instabilities due to water temperature fluctuations and system component vibrations are automatically compensated. In addition, the highest time resolution of the digital oscilloscope can be utilized. Thus, the precision of determination of all the components in Eq. (2.1) was enhanced.

It can be shown from the Christoffel equation (1.1) that the shear wave is more sensitive to stress than the longitudinal wave. This is demonstrated in Fig. 2.3 where velocity sensitivity to stress ($\partial V/\partial\sigma_{11}$) is given as a function of the propagation angle in the 1–3 plane. Thus, precision of stress determination is defined mostly by the precision of the shear wave velocity. The next section discusses the phase correction required for the shear wave velocity measurement after the first critical angle.

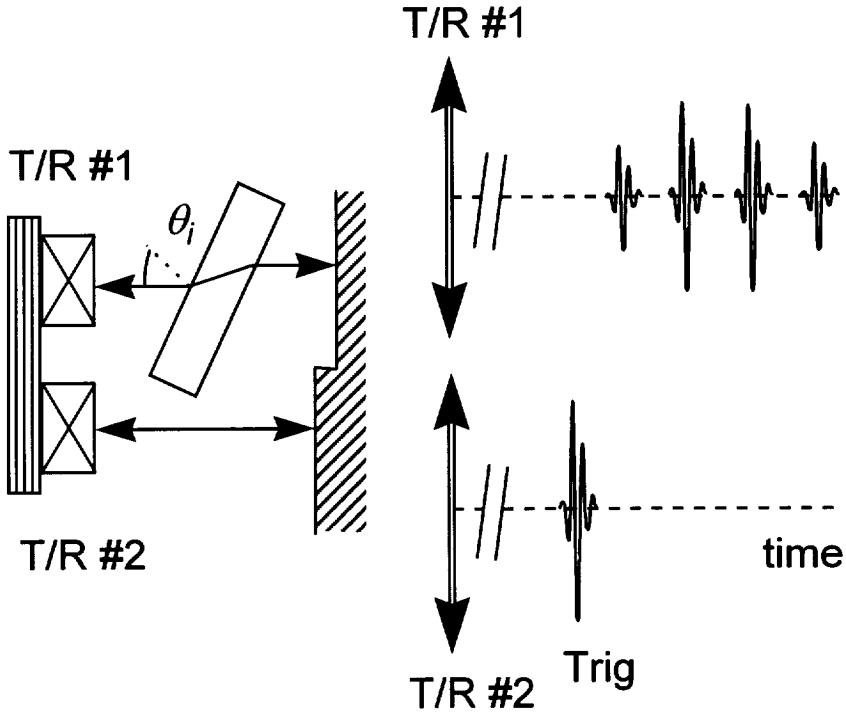

Figure 2.2: Schematic diagram of the two-transducer experimental set-up for self-reference bulk wave velocity measurement.

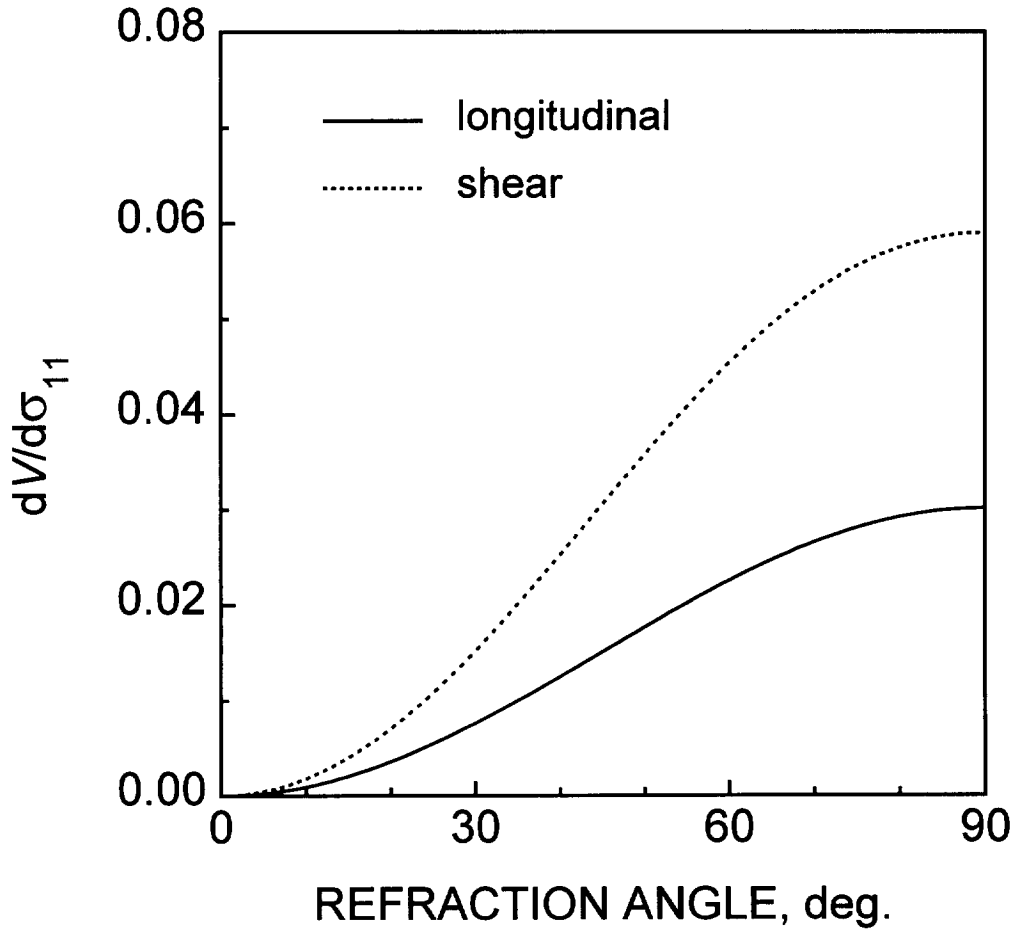

Figure 2.3: Velocity sensitivity to the applied stress σ_{11} as a function of refraction angle.

2.2.1 Phase Correction for Shear Wave

An ultrasonic wave transmitted through a water/solid interface generally converts into a quasi-longitudinal and two quasi-shear waves. After the first critical angle the shear waves have phase shifts due to the presence of the evanescent longitudinal wave near the interface. The effect is demonstrated in Fig. 2.4 on the example of the SCS/Ti matrix composite. Fig. 2.4a shows the amplitude of the shear wave transmitted through the solid/water interface as a function of the incident angle. The corresponding phase shift is shown in Fig. 2.4b. This results in an additional time delay (Fig. 2.5a). We used the following method to correct the measured experimental data. At first wave velocity is calculated from the measured time delays using Eq. (2.1) with no corrections. Then the elastic constants are calculated in the first approximation without taking stress and phase shift into account using the least squares approximation method (Eq. 1.7). Based on the elastic constants found, we calculate the phase shift for the shear wave. Finally, we calculate the phase velocity using both experimental and phase shift data. The procedure can be repeated to improve the precision of the velocity. The shear wave velocity correction is the most significant after the first critical angle which is demonstrated in Fig. 2.5b.

2.3 Experimental Procedure

As an example of method application, the angular dependence of the bulk wave velocity in the plane of symmetry of the plexiglass sample (6.5in.×1in.×3/8in.) was measured at several levels of applied stress. An Alcoa aluminum stressing fixture was used to apply a load to the specimen. The fixture is an aluminum ring which keeps the sample under tension. The ring is calibrated by measuring the compressive

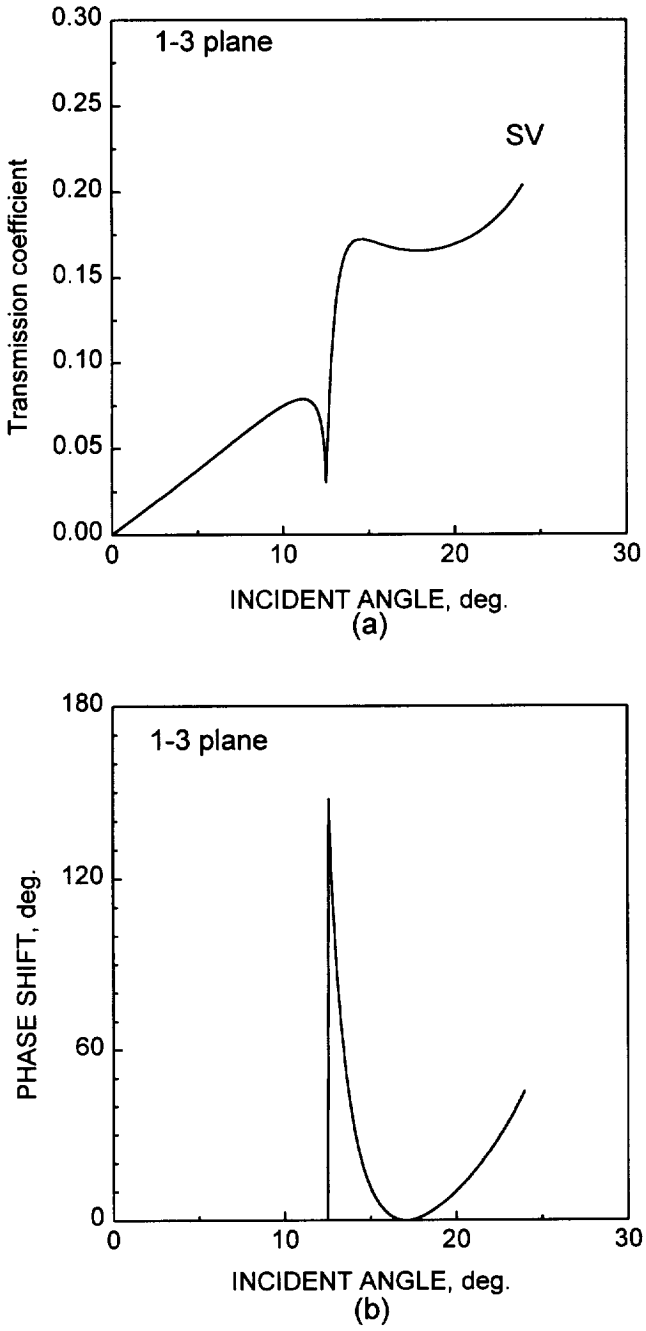

Figure 2.4: Effect of phase shift for the converted shear wave after the first critical angle calculated for the SCS/Ti matrix composite in 1–3 plane. a) Amplitude of the shear wave transmitted through the water/solid interface, b) corresponding phase shift of the shear wave.

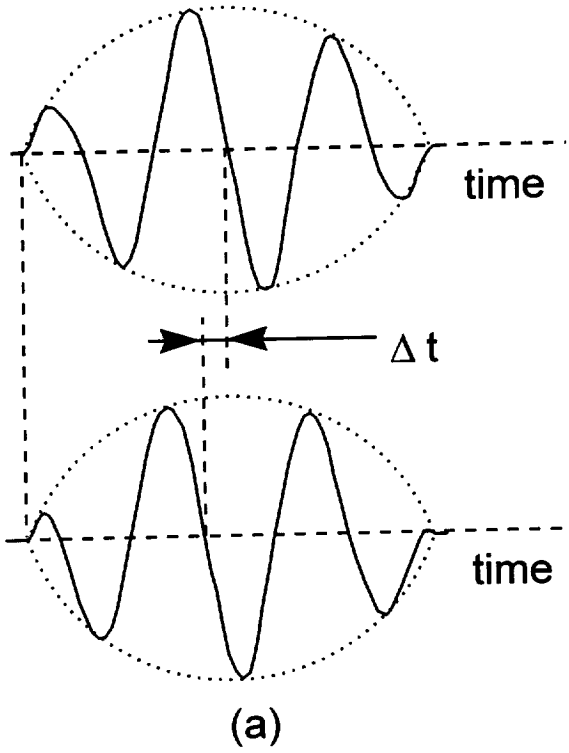

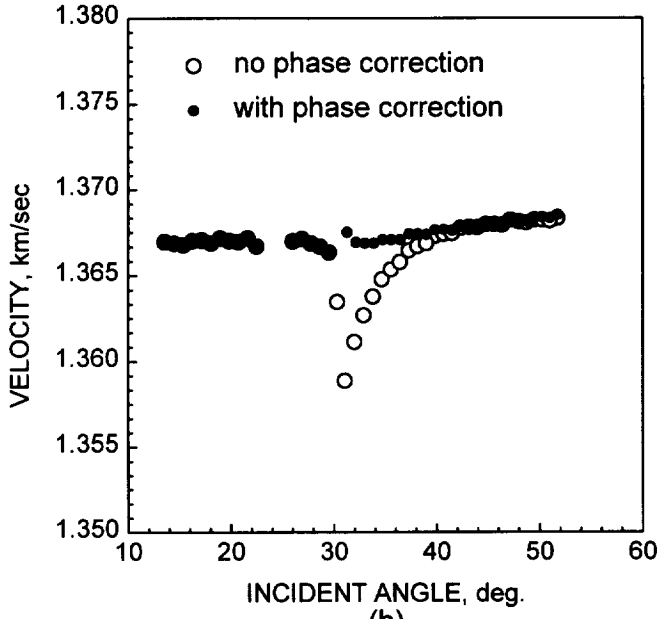

Figure 2.5: a) Schematic of a time delay caused by phase shift of the shear wave passing through the water/solid interface. b) Measured shear wave velocity angular dependence with and without phase correction in plexiglass.

force necessary to reduce the diameter of the ring in the direction of an equal tensile force imposed on the sample. The applied load was measured as ring deflection by a dial indicator, and then the deflection value was converted to a load value using a stressing fixture calibration curve. The precision of the stress applied by a stressing fixture was estimated for a given sample by a strain gage as ± 1 MPa.

To ensure independence of the velocity measurement at different applied stresses we used the following procedure. The sample was placed in the Alcoa ring fixture and loaded. Then the fixture was placed in the experimental setup and necessary adjustments made. After velocity measurements were made the fixture was taken out of the setup and the sample was unloaded. The full procedure was repeated for each applied stress, thus each measured velocity angular dependence and the reconstructed elastic constants and stress were independent.

2.4 Experimental Results

Figs. 2.6(a,b) show the results for longitudinal and shear waves in the plexiglass sample at different applied stresses. One can see the gradual velocity decrease with applied stress; the angular dependence changes as well.

The absolute stress levels were determined from the velocity data using the inversion technique discussed in the theoretical section. The comparison of the applied and reconstructed (from the velocity data) stresses is shown in Table I. One can see that all of the reconstructed stresses are somewhat higher than the applied stresses. For example, for zero applied stress the reconstructed absolute stress is around 3 MPa. All experimental points can be fitted by a dependence $\sigma_{11}^{abs} = \sigma_{11}^{app} + 4\,\mathrm{MPa}$. Since the method is sensitive to the total stress present in the specimen (residual plus applied)

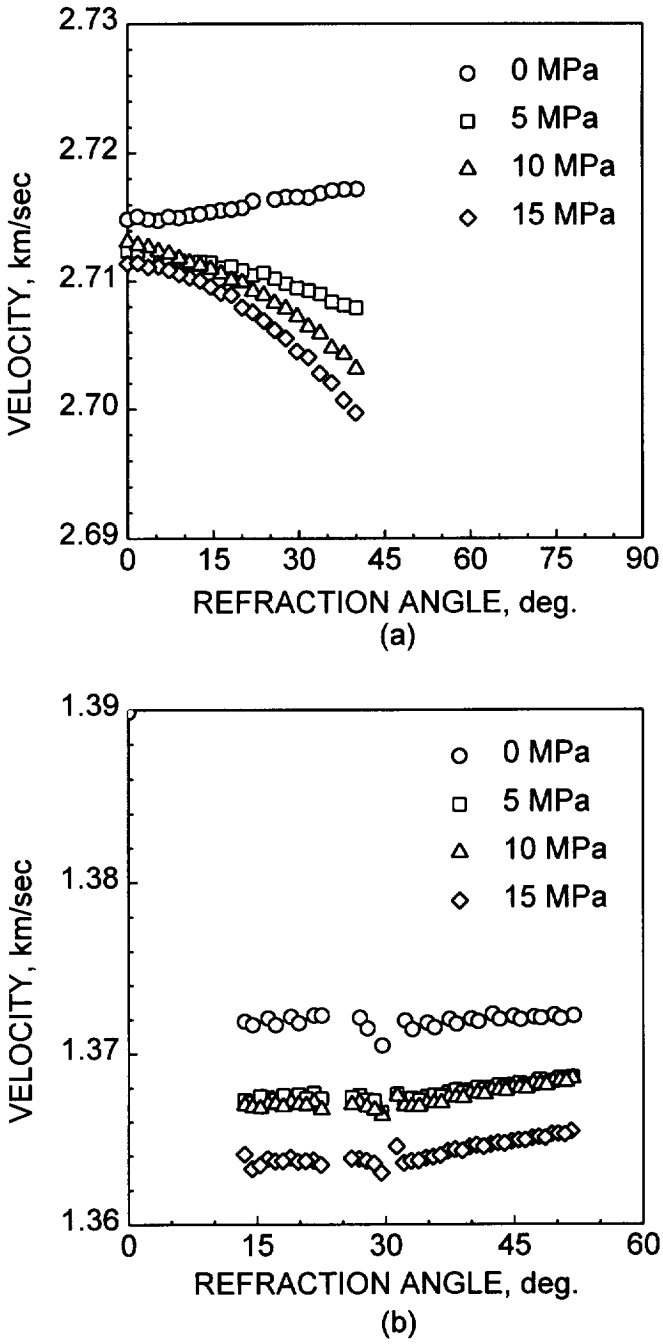

Figure 2.6: Angular dependence of the a) longitudinal and b) shear wave velocity in the plane of symmetry of the plexiglass sample.

Table I: Comparison of applied and reconstructed-from-the-velocity-data unidirectional stress in plexiglass.

Reconstructed stress, MPa	Sample stress after subtraction of the residual stress of 4 MPa	Applied stress, MPa
3	-1	0
11	7	5
15	11	10
17	13	15

we conclude that the given specimen has a residual stress of around 4 MPa. The absolute error in stress determination is about 2 MPa; it is evaluated numerically using the estimated random experimental error in the absolute velocity measurements (about 0.3%). Future experiments are needed to establish the applicability of the technique described for more practical cases.

2.5 Conclusions

An experimental technique for absolute stress determination from angular dependence of ultrasonic velocities has been introduced. Preliminary experimental stress determination has been done in a homogeneous specimen at different applied stress levels using a modified Self Reference Bulk Wave (SRBW) technique for the ultrasonic velocity measurements. The technique was modified to improve velocity measurements: 1) introduction of a second transducer with wave path through water and 2) phase correction of the shear wave transmitted though the specimen. Each velocity mea-

surement has been performed with independent sample alignment and stressing. The stress is determined from inversion of the Christoffel equation in a multidimensional space formed by the stress dependent elastic constants and the stress components.

Chapter 3

APPLICATION TO DETERMINATION OF RESIDUAL STRESSES IN COMPOSITES

3.1 Introduction

High temperature composites have a potential to provide significant performance improvement and weight reduction in aircraft engines and other structures. For successful application of these materials in different environments their mechanical properties, life capability and reliability must be well known. The high cost of structures engineered from these materials makes experimental life determination very difficult. Thus NDE of such composite structures becomes very important.

The metal matrix (MMC) and intermetallic (IMC) composites are manufactured at elevated temperatures. Due to thermal expansion mismatch between fibers and matrix the residual stresses occur during the material cooling from processing to room temperature. The residual stresses influence the properties of MMC and IMC composites. The levels of these stresses may vary significantly for different constraints, geometries and processing histories in composite structures. These stresses can be sufficiently large to yield the matrix material. They can also lead to matrix cracking and fiber/matrix interface debonding, thus reducing the composite strength. Temperature changes (e.g. in aircraft engines) during service also significantly affect the distribution of the residual stresses. All that can significantly affect the performance of structural parts made from these composites.

A brief review of existing measurement techniques and theoretical models for residual stress assessment in composites is presented in Section 3.2. It shows that there is still a great need for less expensive *in situ* techniques for nondestructive residual stress determination in composites. This makes ultrasonic methods very attractive. It has been demonstrated that ultrasonic wave velocity measurements can be successfully used for characterization of fiber-matrix interphase [11] and fatigue damage [12] in high-temperature composite materials.

The purpose of the present work is to describe quantitatively changes in ultrasonic wave velocities propagating through the composite material with residual stresses to show the feasibility of development of ultrasonic techniques for assessment of residual stresses in composite structures. In order to do that we need to consider wave propagation through the nonhomogeneous medium with nonhomogeneous stress distribution. In Section 3.3 we describe governing equations for a wave propagation in a stressed medium and boundary conditions at the interface between two stressed media. These equations provide a foundation for the description of wave propagation through multilayered stressed structure. The detailed computational procedure for the solution of the refraction/refraction problem at the interface between two generally anisotropic stressed media is given in [17]. Generalized self-consistent multiple scattering model [18, 19] serves as a basis for determination of velocity and attenuation of ultrasonic wave in unidirectional composites with multilayered fibers. We briefly review it in Section 3.4.1. The model allows to consider an arbitrary number of fiber and matrix phases in the analysis of wave dispersion and scattering. Application of the model for determination of velocities in a composite with residual stresses is described in Section 3.4.2. Calculation results for ultrasonic wave velocities in SCS-6/Ti composite with and without residual stresses are presented in Section 3.5. Preliminary results were given in [20].

3.2 Methods of residual stress assessment in high temperature composite materials

With the rapid development of new composite materials in the past three decades significant effort has been put into improving models and techniques for estimating

residual stresses in composites.

Existing measurement techniques for residual stresses utilize X-ray or neutron diffraction. X-ray diffraction ($\sin^2$-psi method) has been successfully applied to SCS - 6 reinforced titanium matrix composites by several groups of researchers [21, 22]. They all obtained comparable results showing significant levels of matrix tension in both fiber and transverse directions, with the fiber direction stresses being higher. More recently neutron diffraction was developed to measure residual stresses, and used for high temperature composites [23]. Lattice strains are determined by measuring the shift in the diffraction peaks for the composite constituents between stressed and stress-free samples. Neutron radiation has the advantage of deep penetration, thus allowing the sensing of both fibers and matrix without destructive polishing.

Modeling of the thermal response in high temperature composites can be performed using analytical concentric cylinder models (CCM) [24, 25] or finite element models (FEM) [26, 27]. Today's models allow us to calculate residual thermal stresses in high temperature composites and to explore the influence of material properties (fibers, matrices, interface coatings) and processing (cooldown history and fabrication temperature). Also, plastic and time-dependent deformations are included in most of these models. The advantage of CCM is computational speed and thus the possibility to perform parametric studies of the influence of fiber and matrix characteristics (fiber morphology, matrix yield strength) and fiber/matrix interface properties on the level of residual stresses. The advantage of finite element analysis is the possibility of studying the effect of fiber packaging and different lamina orientation (i.e. cross-ply). But these calculations require powerful computational resources.

Wright et al. [22] compared CCM, FEM, X-ray and neutron diffraction for different metal matrix composite materials. There is good agreement of model predictions

with measurements by both X-ray and neutron diffraction techniques. However neutron diffraction cannot be used *in situ* during processing, it is extremely expensive and can be performed only in several national laboratories and X-ray diffraction is sensitive to only near surface stresses because of small penetration depth.

Estimation of residual stresses in SCS-6/Ti composite which arise during the cooling process from processing temperature of 815°C to room temperature (23°C) using CCM is presented at Fig. 3.1. We used the local/global matrix formulation of the boundary value problem of an arbitrarily layered concentric cylinder proposed by Pindera et al. [25]. This formulation allows easily to incorporate an arbitrary number of elastoplastic shells with temperature dependent properties into the concentric cylinder. Fiber is considered to have multilayered structure consisting of carbon core, SiC shell and carbon-rich coating (Fig. 3.2a). Fiber volume fraction is 0.24. Temperature dependent elastic properties of Ti matrix are taken from [25]. CCM assumes zero shear stresses, thus only nonzero stress components are axial, radial and hoop (Fig. 3.2b). To satisfy boundary conditions at the interfaces radial stress is considered to be continuous. The continuity of radial displacements is incorporated automatically into the model. According to our calculations Ti matrix yields at 243°C. One can see that the level of residual stresses is high and stress distribution is nonhomogeneous. For example compressional axial stress in SiC shell is around 1000 MPa, while the tensile axial stress in Ti matrix is about 300 MPa. These stress levels lead to plastic deformations and may affect the performance of structural components made from this composite material.

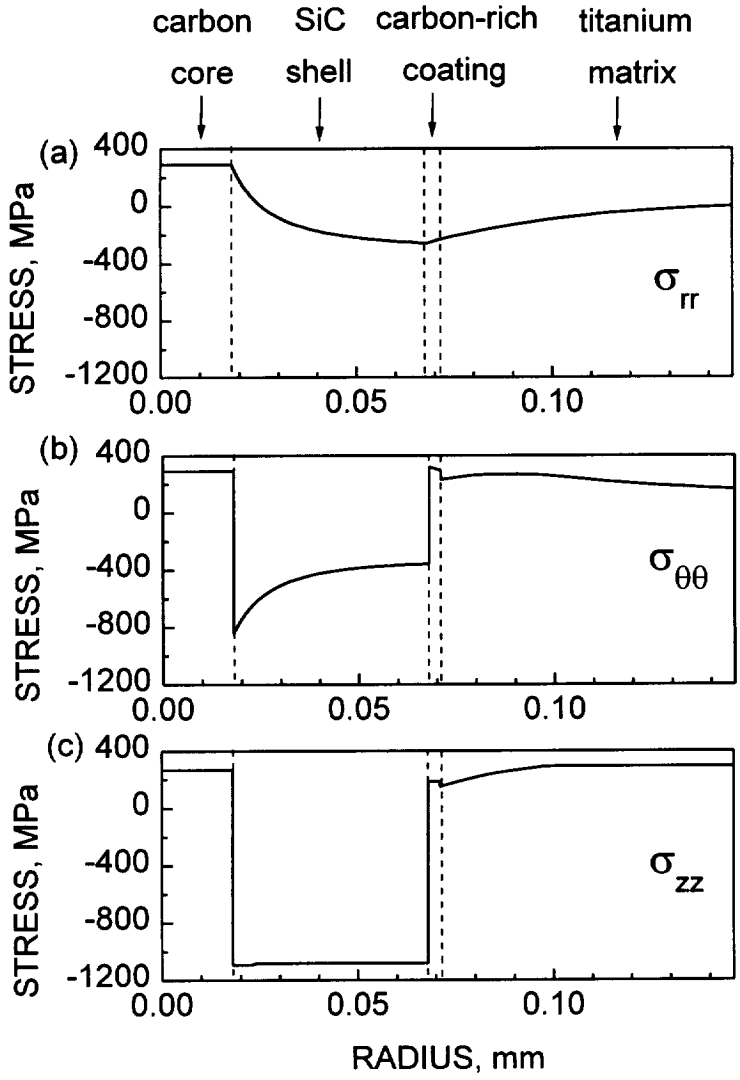

Figure 3.1: Residual stresses in SCS-6/Ti composite due to temperature change of $-792°C$ estimated using concentric cylinder model (CCM).

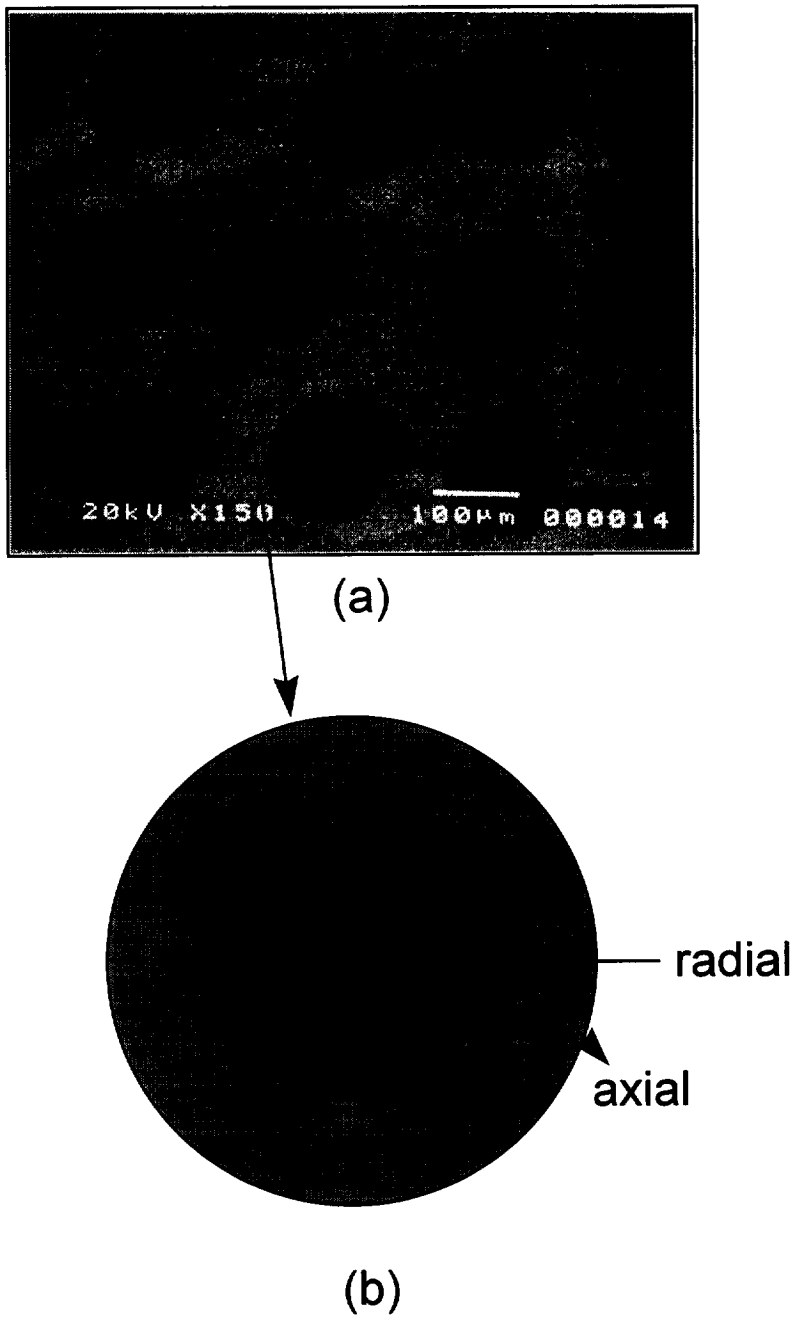

Figure 3.2: SEM photograph of a SCS-6/Ti unidirectional composite sample.

3.3 Wave propagation through a plane interface between two anisotropic stressed media

In this section we present governing equations for a wave in stressed homogeneous layer and boundary conditions at the interface between two stressed layers. These equations will serve as building blocks for modeling of ultrasonic wave propagation through and scattering from multiple interfaces between stressed fiber and matrix layers.

To describe the wave propagation in a prestressed medium the approach proposed by Man and Lu [7] is used. The prestressed configuration is the only reference configuration in this approach and the initial stress is included in the constitutive equation:

$$\sigma_{ij} = \sigma^0_{ij} + C_{ijkl}\epsilon_{kl} + u_{i,k}\sigma^0_{kj}, \ . \tag{3.1}$$

where σ_{ij} is the first Piola-Kirchhoff stress tensor, σ^0_{ij} is the initial static stress, ϵ_{ij} is the elastic strain due to wave propagation, $u_{i,k}$ is the displacement gradient and C_{ijkl} is the fourth rank tensor of stress dependent elastic constants. Eq. (3.1) gives the relation between stresses and displacements which arise due to wave propagation in the prestressed medium. It is an analog of Hook's law for the unstressed case. In general the stress σ_{ij} can be both applied and residual since there is no restriction that the resulting deformation be elastic.

The equation of motion has the following form:

$$\sigma_{ij,j} = \rho\ddot{u}_i. \tag{3.2}$$

Using (3.1), (3.2) can be rewritten as

$$(C_{ijkl} + \sigma^0_{il}\delta_{jk})u_{k,jl} = \rho\ddot{u}_i. \tag{3.3}$$

Now assuming that the material and local (over the size of the transducer) stresses are homogeneous and using a plane wave solution for $\mathbf{u}$

$$u_k = AP_k e^{iK(\mathbf{n}\cdot\mathbf{x}-Vt)} \tag{3.4}$$

where A is the amplitude of the wave, P_k is the unit displacement vector, $\mathbf{K} = K\mathbf{n} = (\omega/V)\mathbf{n}$ is the wave number, $\mathbf{V} = V\mathbf{n}$ is the wave velocity, $\mathbf{n}$ is the wave normal, and $\mathbf{x}$ is the position vector, one has the Christoffel equation for an anisotropic material under stress:

$$[C_{ijkl}n_i n_l + (\sigma^0_{il}n_i n_l - \rho V^2)\delta_{jk}]P_k = 0. \tag{3.5}$$

Eq. (3.5) has nontrivial solutions when the determinant is equal to zero

$$|G_{jk} - \rho V^2 \delta_{jk}| = 0 \tag{3.6}$$

where G is the generalized Christoffel tensor with components

$$G_{jk} = (C_{ijkl} + \sigma^0_{il}\delta_{jk})n_i n_l. \tag{3.7}$$

It can be shown that G is symmetric ($G_{ij} = G_{ji}$) and the eigenvalue problem has three real solutions as for an unstressed medium.

Let us consider a plane interface between two generally anisotropic stressed media. ν is the vector normal to the interface (Fig. 3.3). Index "I" refers to the upper medium and "II" to the lower medium. The initial stresses are $(\sigma^0_{ij})_I$ and $(\sigma^0_{ij})_{II}$ for upper and lower media respectively. For a static stressed state the boundary conditions represent the continuity of the traction forces:

$$(\sigma^0_{ij})_I \ \nu_j = (\sigma^0_{ij})_{II} \ \nu_j. \tag{3.8}$$

Consider a monochromatic plane wave (3.4) propagating from the upper to the lower medium. The boundary conditions at the interface represent continuity of displacements and traction forces. In the general case, for a wave incident from the upper

medium there are three reflected (in upper medium, $\alpha = 1, .., 3$) and three transmitted (in lower medium, $\alpha = 4, .., 6$) waves. The boundary conditions are:

$$\begin{aligned} \mathbf{u}^{inc} + \sum_{\alpha=1}^{3} \mathbf{u}^{\alpha} &= \sum_{\alpha=4}^{6} \mathbf{u}^{\alpha} \\ \sigma_{ik}^{inc}\nu_k + \sum_{\alpha=1}^{3} \sigma_{ik}^{\alpha}\nu_k &= \sum_{\alpha=4}^{6} \sigma_{ik}^{\alpha}\nu_k \end{aligned} \tag{3.9}$$

Using Eq. (3.1) and taking into account static boundary conditions (3.9) each of the terms $\sigma_{ij}\nu_j$ is equal to

$$\sigma_{ij}\nu_j = C_{ijkl}\epsilon_{kl}\nu_j + u_{i,k}\sigma_{kj}^{0}\nu_j \tag{3.10}$$

Note that, in comparison with the boundary conditions for traction forces in the unstressed case, the elastic constants are replaced with stress dependent elastic constants and an additional term $u_{i,k}\sigma_{kj}^{0}\nu_j$ appears. Boundary conditions for displacements are the same as for the unstressed state.

3.4 Multiple scattering models

An ultrasonic bulk wave propagating through the composite averages the properties of the constituents. In order to describe this averaging quantitatively and assess the effect of stresses in constituents on it we need to consider wave interaction with a multilayered structure of a complex geometry.

3.4.1 Generalized Self-Consistent Multiple Scattering Model

Interference of a wave scattered from different fibers in the composite resulted in the scattering induced wave attenuation and dispersion. To calculate the velocities of ultrasonic waves propagating in the direction perpendicular to the fibers in a uniaxial composite a modified Waterman-Truell multiple scattering model [18, 19] is used.

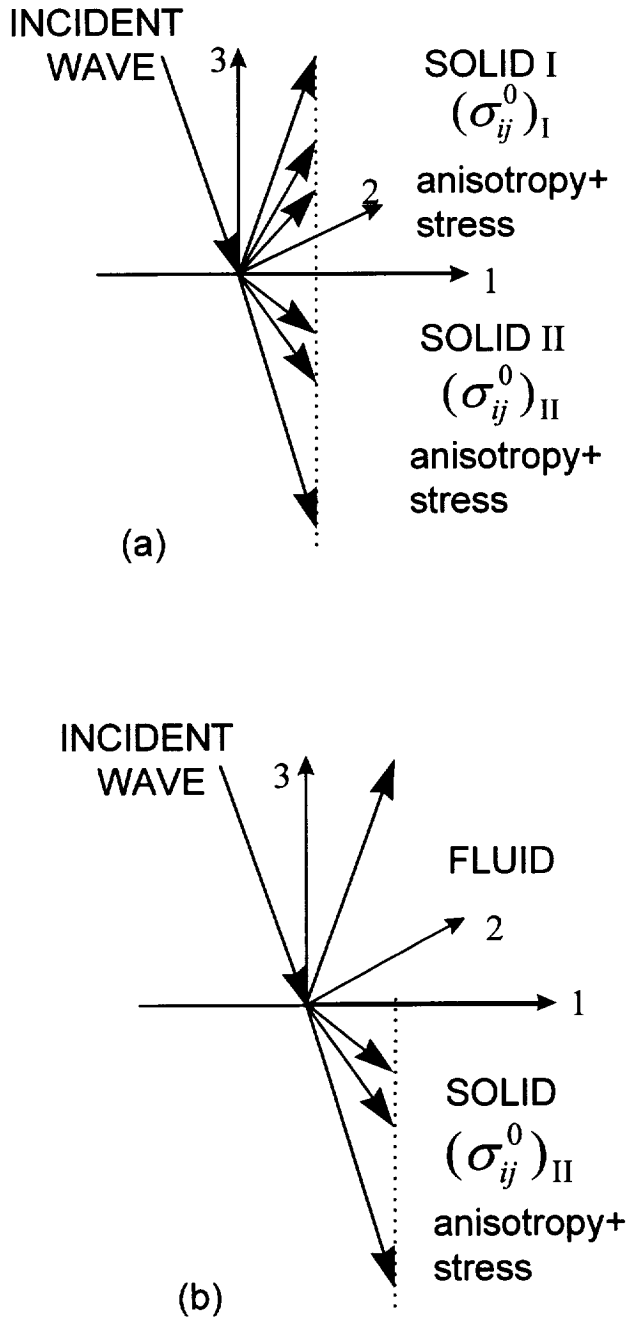

Figure 3.3: Wave propagation through the plane boundary between anisotropic stressed media.

In the Waterman-Truell model [28] the wave number is found by averaging a joint probability distribution over all scatterers. For a unidirectional composite with identical fibers, the multiple scattering field yields a complex wave propagation constant $\beta = \omega/V_c + i\alpha$ as

$$(\frac{\beta}{k})^2 = [1 - \frac{2\, i\, n_s\, f(0)}{k^2}]^2 - [\frac{2\, i\, n_s\, f(\pi)}{k^2}]^2, \tag{3.11}$$

where $n_s = \frac{c}{\pi r_f^2}$ is the number of fibers per unit area, r_f is the fiber radius and c is the fiber fraction; $k = k^m$ is the wave number of the matrix, and $f(0)$ and $f(\pi)$ are the forward and backward scattering amplitudes calculated from a single fiber embedded in a matrix with wave number k as shown in Fig 3.4a. One sees from equation (3.11) that both V_c and α are dependent on frequency.

The solutions (3.11) exhibit low-frequency velocity limits different from those predicted by the well-known static solutions (for example the generalized self-consistent model (GSCM) [29]). To satisfy the correct static limit the Waterman-Truell model could be modified as shown at Fig. 3.4b where the composite cylinder consisting of the multilayered fiber as the core and the matrix material as the annulus is considered embedded in the effective medium. The effective medium properties are the same as those of the composite and assumed to be unknown and have to be determined. The forward and backward scattering amplitudes $f(0)$ and $f(\pi)$ are found for scattering from the composite cylinder by waves incident from the effective medium with wave number k^e and (3.11) is solved in a self-consistent manner which requires $\beta = k^e$. In this way, all the static solutions given in [29] match with the static limits of the longitudinal and transverse wave velocities. This dynamic model was developed by Mal and Yang [30] for study of SH shear wave propagation, and by Huang and Rokhlin [18] for longitudinal and SV shear waves propagation in composites. Fig. 3.5 shows the comparison of experimental results (dots) and theoretical prediction by GSCM

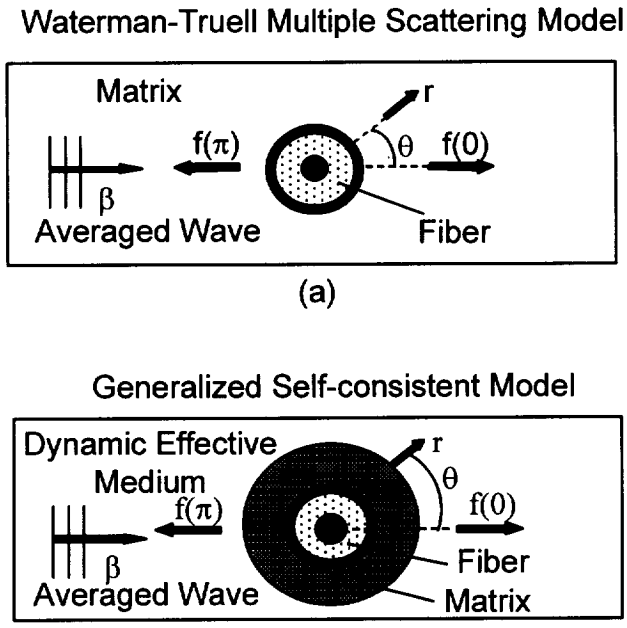

Figure 3.4: (a) Self-consistent and (b) generalized self-consistent multiple scattering models.

Waterman-Truell solution (solid line) for a longitudinal wave propagating perpendicular to fibers in SCS-6/Ti composite. One can see that experiment and theory agree well.

3.4.2 Application of the Model for a Stressed Composite

The above model could be modified and used to estimate wave velocities in the stressed composite. As an example we will consider the 4-phase SiC/Ti composite with residual stress distribution shown at Fig. 3.1.

First stresses are discretized. Each phase is divided into several layers and it is assumed that stresses are constant within each layer taking for the stress level the average of values on the inner and outer boundaries (Fig.3.6). By doing so, a 4-layered system is substituted by $n-1$ layers. Index 1 refers to the fiber core, index $n-1$ represents the outer matrix layer and index n refers to the effective medium. Each layer j is characterized by the elastic properties of the corresponding phase and by three discretized stress components (radial, axial and hoop) which are assumed to be constant through the layer. Each layer is considered to have isotropic properties in the transverse (with respect to the fiber direction) plane. In the presence of residual stresses isotropy is violated since the radial and hoop stresses are different. However radial symmetry still holds. Since elastic field is decomposed to cylindrical waves propagating in the radial direction the multiple scattering mainly depends on the material properties which define velocities of longitudinal and shear waves in radial direction. From the solution of the Christoffel Eq. (3.5) the velocities of the longitudinal and shear waves in the radial direction are:

$$\rho V_l^2 = C_{rr} + \sigma_{rr}^0, \qquad \rho V_s^2 = G_t, \tag{3.12}$$

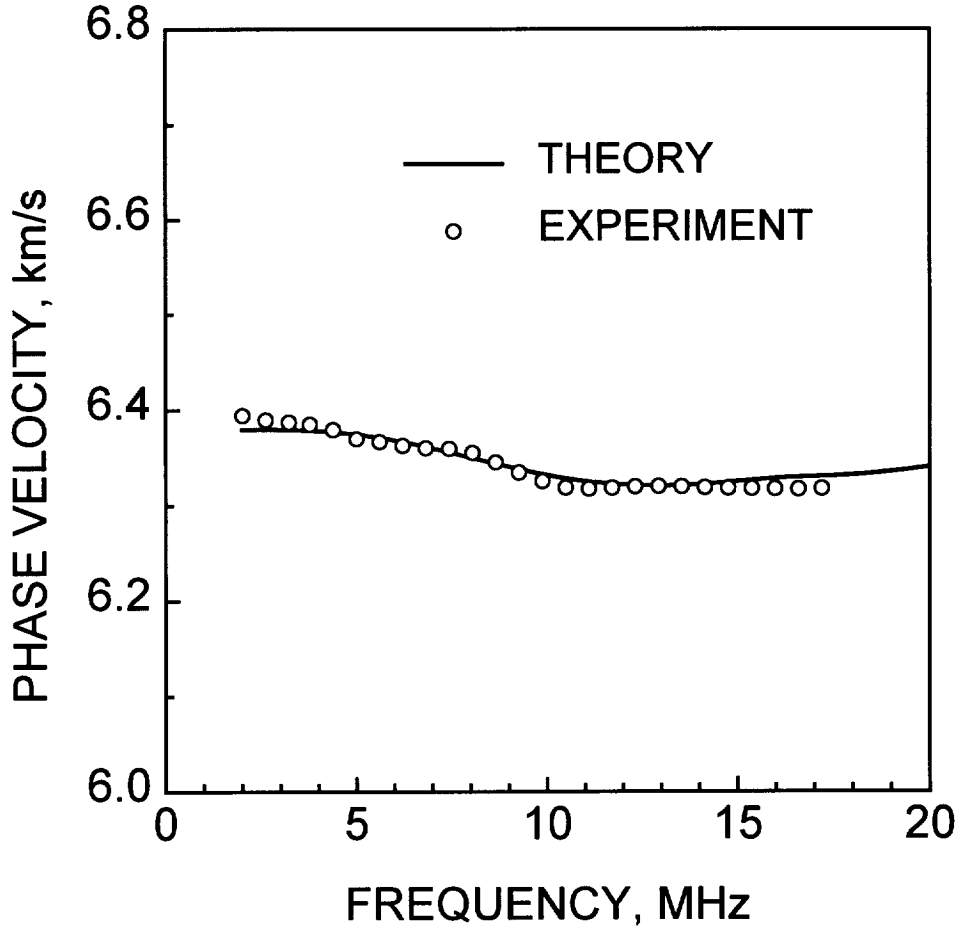

Figure 3.5: Measured and predicted by GSC model frequency dependence of a longitudinal wave in SCS-6/Ti composite.

where C_{rr} and G_t are the radial and transverse shear stress dependent elastic constants and σ_{rr}^0 is the radial component of the residual stress. Stress dependent elastic constants can be determined from second and third order elastic constants and stresses assuming that the deformation is hyperelastic. Formulas for stress dependent elastic constants are presented in [9].

The multiple scattering model described in the previous section assumes isotropy of each layer in the transverse plane. Since most of the scattering occurs within small angular range from radial direction we assume that isotropic moduli for each layer are equal to those which define longitudinal and shear wave velocities (3.12) in the radial direction in the anisotropic actual layer. One can define the effective radial $C_{rr}^{eff} = C_{rr} + \sigma_{rr}^0$ and transverse shear $G_t^{eff} = G_t$ moduli. The effect of residual stresses is included in stress dependent elastic constants C_{rr} and G_t and as a direct stress term σ_{rr}^0 in C_{rr}^{eff}.

Thus, 4-phase composite with residual stresses is approximated by $(n-1)$-layered composite system, where the properties of j-th layer are $(C_{rr}^{eff})_j$ and $(G_t^{eff})_j$. The Generalized self-consistent multiple scattering model described in the previous section can be applied to this system to determine the dispersion of longitudinal and shear (polarized perpendicular to the fiber direction) waves propagating normal to the fibers.

To illustrate that the error in velocities of scattered waves introduced by isotropic approximation is small, we calculated longitudinal and shear wave velocities in the Ti matrix at different propagation angles α with respect to the normal to the fiber direction (Fig. 3.7). Axial stress of 300 MPa, radial stress of 250 MPa and hoop stress of 200 MPa were assumed in the matrix. These are averaged values of residual stresses predicted for the Ti matrix using CCM (Fig. 3.1). The results are presented at

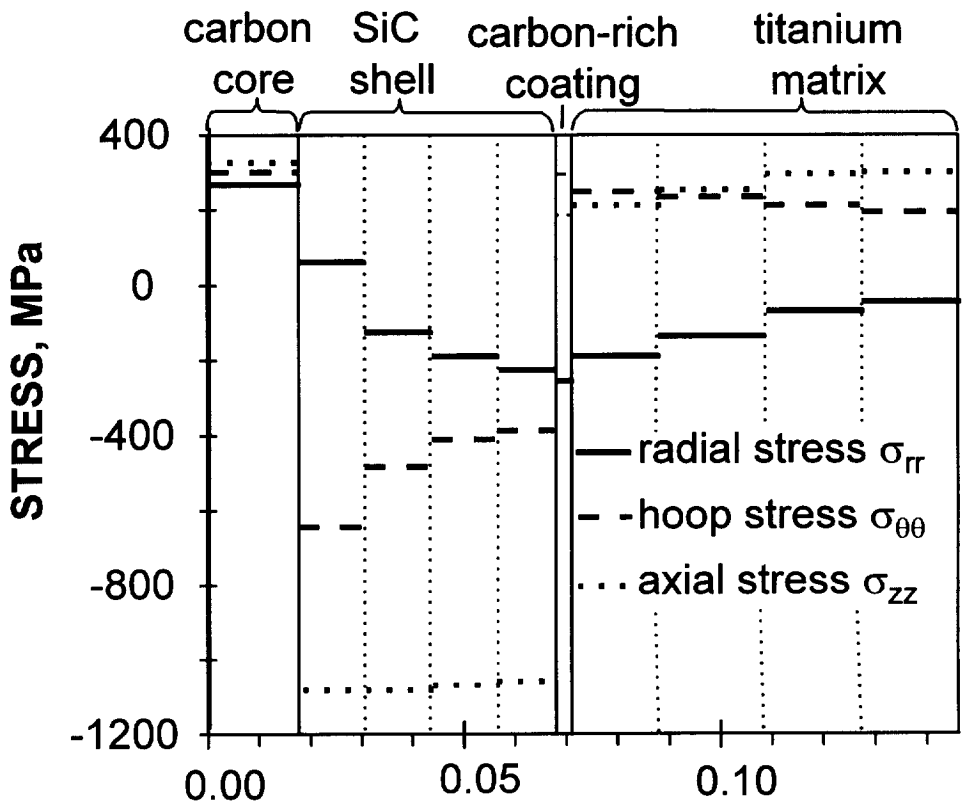

Figure 3.6: Discretization of residual stresses in SCS-6/Ti composite.

Fig. 3.8a,b for longitudinal and shear wave velocities respectively. Dotted line shows velocities in unstressed material, dashed line represents the isotropic approximation for the stressed case (which is described above) and solid line gives the exact velocity value predicted by the acoustoelastic theory (Section 3.3). One can see that in 10° range from the fiber normal the difference between the exact solution and isotropic approximation is only few meters per second for longitudinal wave. For shear wave it is even smaller. Thus, the assumption about isotropic properties of each layer in the transverse plane is reasonable.

3.5 Simulation results

The approach described in the previous section was utilized to determine wave velocity changes due to the presence of thermally induced residual stresses in the 4-phase SCS-6/Ti composite, consisting of carbon core, SiC shell, carbon-reach coating and titanium matrix. The residual stresses were estimated using CCM as described in Section 3.2 are presented in Fig. 3.1. Elastic properties of each phase in the transverse direction are presented in Table I. Third order elastic constants for all fiber phases (core, shell and coating) were taken from the handbook [10] to be those corresponding to Si and for matrix those for Ti. They are given in Table II. For stress discretization the SiC shell and Ti matrix were each split into five layers. The carbon core was left intact because it has constant stresses. The carbon-rich coating is much thinner than the other phases, so it was not split either. Thus the total number of layers was 12.

Wave velocity calculations using the model described in previous section were performed for different frequencies. The results are presented in Fig. 3.9a,b for longitudinal and shear waves propagating in the normal to fibers direction. Shear wave

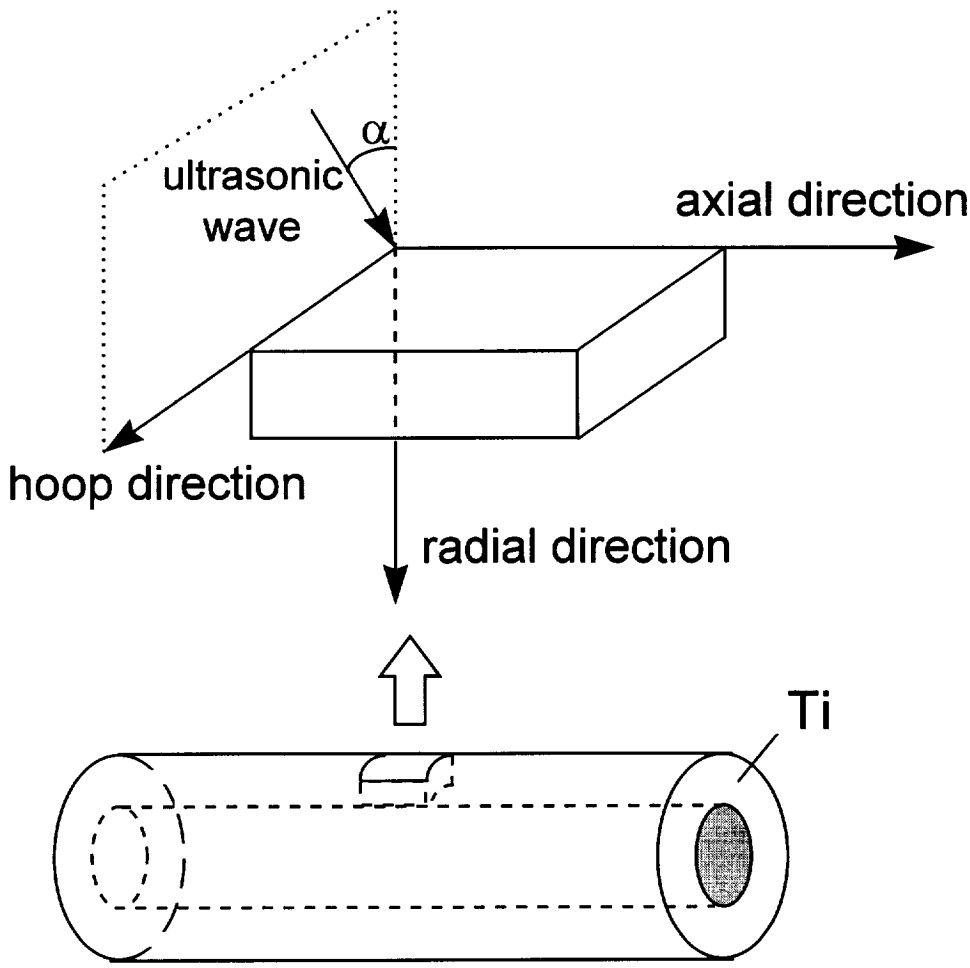

Figure 3.7: Wave propagation in stressed Ti matrix with residual stresses.

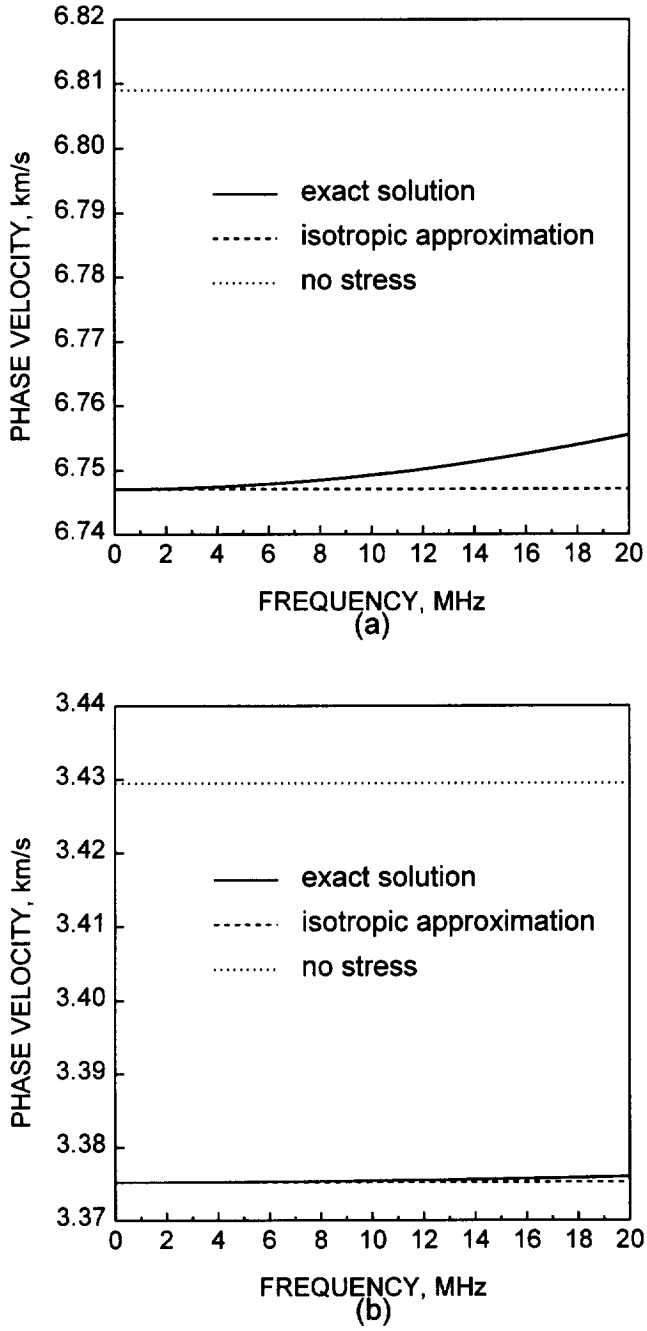

Figure 3.8: (a) Longitudinal and (b) shear wave velocities in Ti matrix without and with residual stresses.

Table I: Transverse properties of each phase in a SCS-6/Ti composite.

phase	C^0_{rr}, GPa	G^0_t, GPa	ρ, g/cc	r, μm
core (carbon)	49	16	1.7	18
shell (SiC)	446	177	3.2	68
interphase (carbon-reach coating)	31	4.6	2.1	71
matrix (titanium alloy)	193	45	5.4	146

Table II: Third order elastic constants for Ti and Si.

material	C_{111}, GPa	C_{112}, GPa	C_{123}, GPa
Ti	-1358	-1105	-162
Si	-821	-448	-104

is polarized perpendicular to fiber direction. Five cases are considered: unstressed composite (dashed line), the case when only axial stresses (dotted line) in matrix and fiber are accounted for, the case when stresses are considered in matrix and residual stress in fiber is zero (dash-dotted line), and when stresses only in fibers are accounted for (dash-double-dotted line). Finally the effect of all residual stresses is taken into consideration (solid line). One can see that the changes in velocities due to the presence of stresses are of order 1%.

3.6 Summary

A numerical procedure has been developed to determine velocities of ultrasonic waves propagating through the composites with residual stresses. The procedure is based on

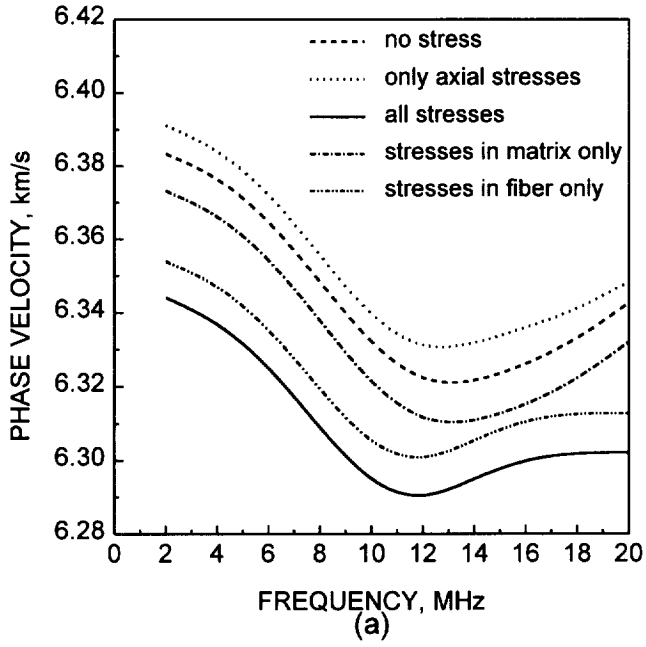

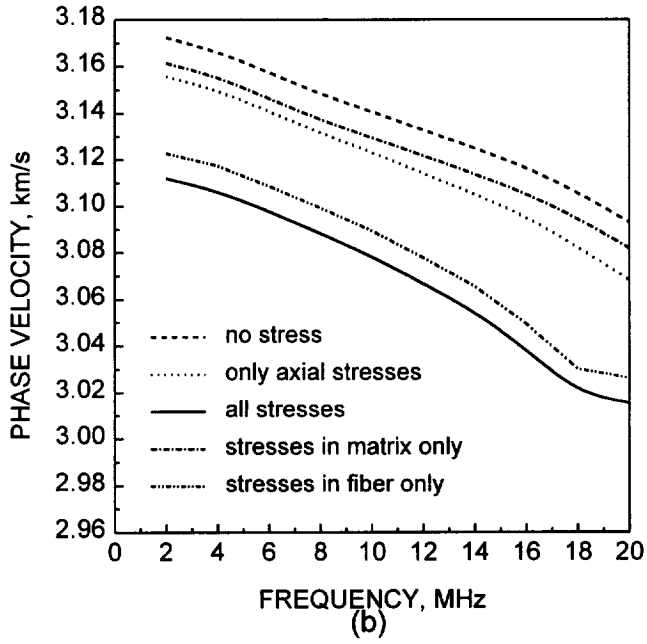

Figure 3.9: Longitudinal (a) and shear (b) wave velocities in the perpendicular to fibers direction in SCS-6/Ti composite with and without residual stresses.

the modified generalized self-consistent model. The model accounts for multiple wave scattering and multilayered structure of the composite. Simulation results performed for SCS - 6/Ti metal matrix composite show that changes in the longitudinal and shear waves in the perpendicular to fibers direction are about 0.5% and 2.0% respectively.

Bibliography

[1] Y. H. Pao, W. Sachse and H. Fukuoka, in *Physical Acoustics*, Vol. 17, eds. W. P. Mason and R. N. Thurston (Academic, New York, 1984), Chap.2.

[2] J. H. Cantrell and K. Salama, "Acoustoelastic characterization of materials", International Materials Reviews **36**, 125-145 (1991).

[3] R. B. Thompson, W.-Y. Lu and A. V. Clark, Jr., in *Handbook of Mesurements of Residual Stresses*, Ed. J. Lu, (Fairmont Press, Lilburn, 1996).

[4] R. B. King and C. M. Fortunko, "Determination of in-plane residual stress in plates using horizontally polarized shear waves," J. Appl. Phys. **54**, 1339-1354 (1983).

[5] Y. Iwashimizu and O. Kobori, "The Rayleigh wave in a finitely deformed isotropic elastic material," J. Acoust. Soc. Am. **64**, 910-916 (1978).

[6] R. B. Thompson, S. S. Lee and J. F. Smith, "Angular dependence of ultrasonic wave propagation in a stressed, orthorombic continuum: theory and application to the measurement of stress and texture," J. Acoust. Soc. Am. **80**, 921-931 (1986).

[7] C.-S. Man and W. Y. Lu, "Towards an acoustoelastic theory for measurement of residual stress," J. Elasticity **17**, 159-182 (1987).

[8] T. Tokuoka and Y. Iwashimizu, "Acoustical birefringence of ultrasonic waves in deformed isotropic elastic materials," Int. J. Solids Structures **4**, 383-389 (1968).

[9] A. D. Degtyar and S. I. Rokhlin, "Absolute stress determination in orthotropic materials from angular dependences of ultrasonic velocities," J. Appl. Phys. **78**, 1547-1556 (1995).

[10] Landolt-Börnstein, em Numerical Data and Functional Relationships in Science and Technology (Springer, New York, 1979), Vol. III/11.

[11] Y. C. Chu and S. I. Rokhlin, "Effective elastic moduli of fiber-matrix interphases in high-temperature composites," Metall. Trans. A, **27A**, 165-182 (1996).

[12] S. I. Rokhlin, Y. C. Chu and W. Huang, "Ultrasonic evaluation of fatigue damage in metal matrix composites," Mech. Mater., **21**, 251-263 (1995).

[13] S. I. Rokhlin and W. Wang, "Double through-transmission bulk wave method for ultrasonic phase velocity measurement and determination of elastic constants of composite materials," J. Acoust. Soc. Am. **91**, 3303-3312 (1992).

[14] Y. C. Chu and S. I. Rokhlin, "Stability of determination of composite moduli from velocity data in planes of symmetry for weak and strong anisotropies," J. Acoust. Soc. Am. **95**, 213-225 (1994).

[15] Y. C. Chu, A. D. Degtyar and S. I. Rokhlin, "On determination of orthotropic material moduli from ultrasonic velocity data in nonsymmetry planes," J. Acoust. Soc. Am. **95**, 3191-3203 (1994).

[16] Y. C. Chu and S. I. Rokhlin, "Comparative analysis of through-transmission ultrasonic bulk wave methods for phase velocity measurements in anisotropic materials," J. Acoust. Soc. Am. **95**, 3204-3212 (1994).

[17] A. D. Degtyar and S. I. Rokhlin, "Stress effect on ultrasonic wave propagation through the solid-solid and liquid-solid plane interface," in Review of Progress in Quantitative NDE, Vol. 16, D. O. Thompson and D. E. Chimenti, Eds. (Plenum Press, N.Y., 1997) pp. 1699-1706.

[18] W. Huang and S. I. Rokhlin, "Frequency dependencies on ultrasonic wave velocity and attenuation in fiber composites. Theory and experiments," in Review of Progress in Quantitative NDE, Vol. 14, D. O. Thompson and D. E. Chimenti, Eds. (Plenum Press, N.Y., 1995) pp. 1233-1238.

[19] W. Huang, S. I. Rokhlin and Y. J. Wang, "Effect of fiber-matrix interphase on wave propagation along, and scattering from, multilayered fibers in composites. Transfer matrix approach," Ultrasonics **33**, 365-375 (1995).

[20] A. D. Degtyar, W. Huang and S. I. Rokhlin, "Wave propagation in stressed composites," in Review of Progress in Quantitative NDE, Vol. 15, D. O. Thompson and D. E. Chimenti, Eds. (Plenum Press, N.Y., 1996) pp. 1669-1676.

[21] N. Jayaraman and P. Rangaswamy, "Residual stresses in Ti3Al-SCS-6 fiber reinforced metal matrix composites" Air Force Laboratory WL-TR-91-4020, February 1991, pp. 522-531.

[22] P.K. Wright, M.D. Sensmeier, D. Kupperman and H.Wadley (1991) "Thermal stress effects in intermetallic matrix composites," HITEMP Review 1991, NASA Conference Publication 1991, pp. 45-1 to 14.

[23] S. Majumdar, J. P. Singh, D. Kupperman and A. D. Krawitz, "Application of neutron diffraction to measure residual strains in various engineering composite materials," Trans. ASME: J. Eng. Mater. Technol. **113**, 51-59 (1991).

[24] Y. Mikata and M. Taya, "Stress field in a coated continuous fiber composite subjected to thermal-mechanical loadings", Journal of Composite Materials **19**, 554-578 (1985).

[25] M-J. Pindera, A. D. Freed and S. M. Arnold, "Effects of fiber and interfacial layer architectures on the thermoplastic response of metal matrix composites," NASA Technical Memorandum 105802, August 1992.

[26] R. P. Nimmer, "Fiber-matrix interface effects in the presence of thermally induced residual stresses," ASTM Journal of Composites Technology and Research **12(2)**, 65-75 (1990).

[27] S. M. Arnold, V. K. Arya and M. E. Melis, "Elastic/plastic analyses of advanced composites investigating the use of the compliant layer concept in reducing residual stresses resulting from process," NASA TM 103204, September 1990.

[28] P.C. Waterman and R. Truell, "Multiple scattering of elastic waves," J. Math. Phys., **2**, 512-537 (1961).

[29] R.M. Christensen, "Mechanics of Composite Materials," 2nd edition, Krieger Publishing, Malabar, FL (1991).

[30] A.K. Mal and R.B. Yang, "The influence of fiber-matrix interfacial properties on wave characteristics in metal matrix composites," in Review of Progress in Quantitative NDE, Vol. 13, D. O. Thompson and D. E. Chimenti, Eds. (Plenum Press, N.Y., 1994) pp. 1453-1460.